Superconductivity 8 (2023) 100062

Contents lists available at ScienceDirect

Superconductivity

journal homepage: www.elsevier.com/locate/supcon

Full Length Article

Oxidation in Ca/K-1144 iron-based superconductors polycrystalline compounds

Zuhawn Sung [a], Anastasiya Duchenko [b], Giuseppe Celentano [c], Jaeyel Lee [a], Xiaobing Hu [d,e], Nicola Pompeo [b], Francesca Varsano [f], Andrea Masi [c,*]

[a] Fermi National Accelerator Laboratory, Batavia, IL 60510, USA
[b] Università degli Studi Roma Tre, Dipartimento di Ingegneria Industriale, Elettronica e Meccanica, Via Vito Volterra 62, 00146 Roma, Italy
[c] ENEA, C.R. Frascati, Via Enrico Fermi 45, 00044 Frascati, Italy
[d] Department of Materials Science and Engineering, Northwestern University, Evanston, IL 60208, USA
[e] The NUANCE Center, Northwestern University, IL 60208, USA
[f] ENEA, C.R. Casaccia, Via Anguillarese 301, 00123 Roma, Italy

ARTICLE INFO

Keywords:
Grain boundaries
Superconductivity
Oxidation
Microstructure
Iron based superconductors

ABSTRACT

Iron-based superconductors (IBSCs) are a class of material under investigation for the development of superconducting wires in the low-temperature-high magnetic fields power application. Among the various families of IBSCs, the 1144 $CaKFe_4As_4$ compound is a promising material able to achieve outstanding superconducting properties with a cheap and simple chemical composition. Oxidation, in these compounds, is considered an obstacle for high intergranular critical current density, $J_{c,GB}$. A study devoted to the evaluation of oxidation phenomena and their effects on the superconducting properties is thus needed in order to fully understand the involved mechanisms. From the evaluation of polycrystalline samples obtained by a mechanochemically assisted synthesis route, a degradation of the critical temperature and critical currents has been observed concurrently with oxygen accumulation at grain boundaries in open porosities. However, the crystalline structure at an atomic level seems not affected, as well as intragranular superconducting properties assessed by means of calorimetric methods. These results suggest that loss of superconducting properties in Ca/K-1144 compounds following oxidation is significantly associated with the worsening of grain connectivity.

1. Introduction

Iron Based Super Conductors (IBSCs) constitute a class of material that has recently started to fully unveil its potential for power applications at low temperature and high magnetic fields [1] thanks to the extremely high magnetic critical fields (up to 100 T at liquid helium temperature) and the possibility to produce wires through easily scalable methods such as the Powder in Tube (PIT) technique [2]. Among IBSCs compounds, the compounds from the 122 family – characterized by the $A_xAE_{1-x}Fe_2As_2$ chemical composition (A = Alkaline and AE = Alkaline-Earth) – have attracted most of the interest in this sense, showing the best performance and easiness of production [3]. Implementation of such wires is however still limited by two factors affecting their properties: the need of coherent orientation between the crystallites and the presence of current-blocking impurities at grain boundaries [2]. While the first element is commonly addressed through optimization of mechanical and thermal processes (e.g. [4,5]), grain boundary composition can be modulated via the addition of further elements [6] and it is commonly related to the presence of oxygen contamination [7].

The 1144 family ($AAEFe_4As_4$) [8] constitute a relatively novel class of IBSC characterized by critical temperature of approximately 35 K. This structure is characterized by a rigid alternation of A and AE layers between Fe-As planes, giving rise to a series of intrinsic defects that promote high critical current densities in single crystals [9]. Among this family, Ca/K-1144 compounds are composed by cheap and abundant elements, making this material a promising candidate to produce wires and tapes. The performance obtained by 122 wires has not been equaled so far, with optimization needed on several aspects that include the material synthesis in order to avoid contamination of secondary phases [10–12]. A significant role in this sense can be played by the effect of oxidation on this material, not addressed so far. The

* Corresponding author.
E-mail address: andrea.masi@enea.it (A. Masi).

https://doi.org/10.1016/j.supcon.2023.100062
Received 18 July 2023; Revised 7 August 2023; Accepted 14 August 2023
Available online 19 August 2023

assessment of the effect of oxidation on microstructural and superconducting properties represents thus a needed step to enable these materials for applications.

In our previous works, we developed a mechanochemically assisted synthesis route of Ca/K-1144 polycrystalline compounds [13]. The resulting materials are formed by sub-micron sized grains, leading to a network of grain boundaries that allows an effective assessment of the effect of oxidation on the compound's materials and superconducting properties. In this work we submit the material to different oxidative conditions and observe the effect on the compound by assessing micro-structural variation though scanning electron microscopy (SEM), transmission electron microscopy (TEM) and scanning TEM down to the atomic level. The observed variations are correlated to the superconducting behavior studied by means of resistive, magnetic, and calorimetric techniques.

2. Experimental

The synthesis of the compound has been carried out similarly as in our previous works [14], exploiting a mechanochemical step followed by a thermal treatment at 700 °C. An average volumetric density of 4.1 g/cm^3 was obtained for the various pellets, corresponding to approximately a 79% density with respect to the theoretical value. The sample were oxidized by exposition to air at ambient conditions (average humidity concentration of 3% vol) at different exposure time, as described in the following text. To compare the effect of the oxidizing atmosphere, the material was exposed in pure oxygen for 3 months in a sealed vial.

Electric resistance curves were acquired as a function of temperature via a standard four contacts method, placing the contacts on the edges of the disk-shaped pellets. The critical temperature (T_c) value was determined as the zero-resistance temperature. A 9 T PPMS (physical property measurement system) was used to acquire magnetic hysteresis loops at 4.2 K with the applied external magnetic field normal to the sample disk surface. An estimation of the critical current density was carried out according to the Bean's model [15] from the magnetic hysteresis loops as $J_c = 30 \cdot \Delta M/d$, where ΔM is the difference between the upper and lower magnetization branches, in the conservative assumption of the current flowing across the whole sample. Specific heat (SH) curves were obtained in a 14 T PPMS on small sample fragments by cooling down to 4 K with and without an external applied magnetic field.

Surface and cross-sectional microstructural characteristics were evaluated with Thermofisher Helios 5 CX, dual beam system (field emission scanning electron microscope and Ga ion focused ion beam) equipped with an Oxford Instrument, Xplore X-ray energy dispersive spectroscopy (EDS). Compositions of the sample was analyzed with Oxford Instrument Aztec® software. Microstructural and chemical analysis were performed on an aberration corrected JEOL ARM 200CF microscope. Bright field transmission electron microscopy (TEM) imaging was carried out to observe morphology of oxidized structure, and atomic resolution high angle angular dark field (HAADF) imaging was performed for revealing the atomic lattice structure. Electron transparent foils were prepared by Focused Ion Beam (FIB) using lift-out technique after capping the sample surface with a Pt protective layer.

3. Results

To evaluate the response of the material properties towards oxidation, resistance measurements as a function of the temperature were carried out to assess the critical temperatures (T_c) of the compounds exposed to air for different time. The curves are reported in Fig. 1 (a), normalized at 273 K to highlight the different normal state behavior. The residual resistance ratio (RRR) at 40 K (R_{273K}/R_{40K}) decreases

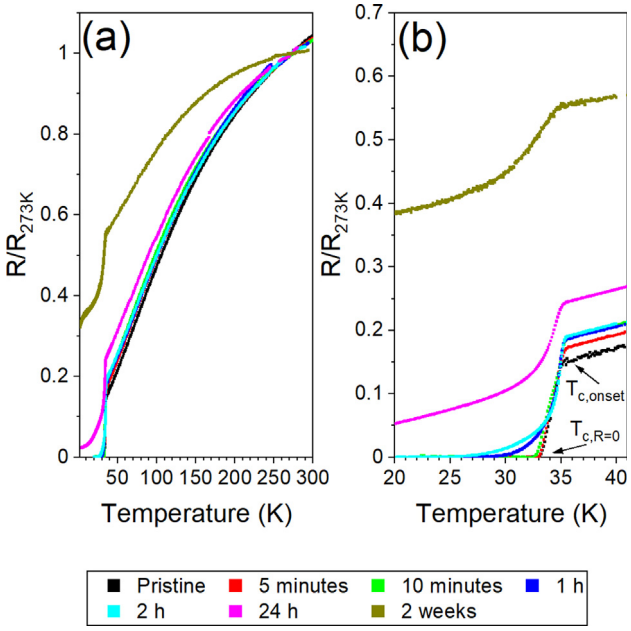

Fig. 1. Resistance as a function of temperature for samples subjected to different air exposure (a) and enlarged view of the superconducting transition (b).

with increasing air exposure. RRR values vary from values higher than 5.5 for fresh samples, to values lower than 2 for samples characterized by high degree of exposure, suggesting a general worsening of grain coupling/connectivity.

At low temperature, all samples exhibit a superconducting transition, as highlighted in Fig. 1(b). The onset (evaluated as the temperature value when the curve starts to deviate from the high temperature linear behavior, $T_{c,onset}$) is similar for all the samples, above 35 K. This suggests that oxidization due to ambient air exposure may not lead to a disordering in the superconducting phases. However, the zero resistance value ($T_{c,R=0}$) decreases from approximately 33 K for the pristine sample to values lower than 25 K for samples exposed for approximately 1 h, and no zero-resistance state is observed for longer exposure times. It is clear thus the detrimental role that air exposure has on superconducting properties of polycrystalline Ca/K-1144 samples.

To evaluate oxidization phenomenon, a detailed microstructural investigation was carried out, starting with the thorough characterization of the pristine compound by means of SEM with EDS analyses. The microstructure of the surface of a freshly synthesized pellet is shown in Fig. 2. It can be observed that the surface of the sample is composed of dense islands surrounded by open porosities, with large crystals growing on the surface. It is straightforward to identify these dense islands with aggregates of sub-micro crystallites, originated following the milling treatment, as already observed by microscopies of fractures of similar samples [16]. Regarding the large crystals, EDX analysis and EBSD measurements [supplementary data] confirm that the chemical composition is compatible with the Ca/K-1144 compound.

To highlight the structure of the bulk, sample cross sections were obtained by FIB processing. An example is reported in Fig. 3a, where it can be observed the cut on the sample surface, protected by a deposited platinum (Pt) layer (light gray on the top). Secondary electron through-the-lens (TTL) detecting image presents clear contrast variation among segregated particles, aggregate grain boundaries, and voids. Red arrows indicate the aggregated grain boundaries. The sample cross section resembles what expected from fractures [13,16], with dense aggregates surrounded by more porous zones. EDX mapping of the examined cross section is reported in Fig. 3b. Further SEM/EDS

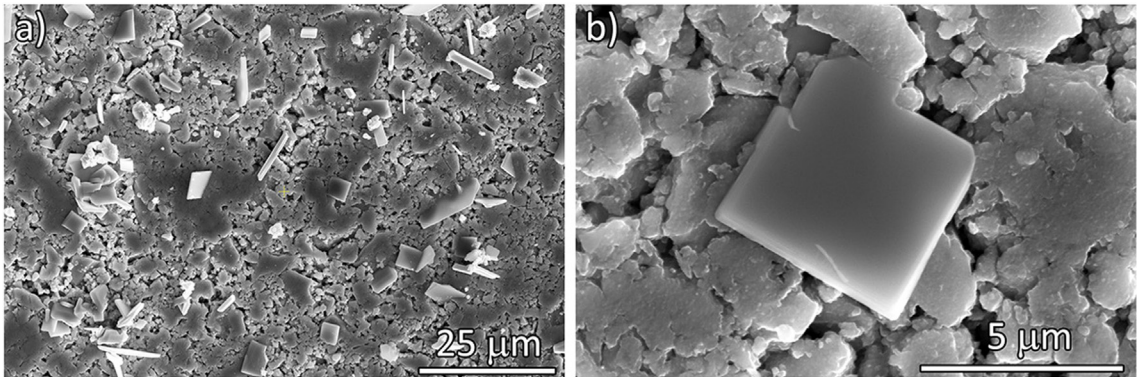

Fig. 2. SEM images of the surface of a freshly synthesized pellet. a) low magnification and b) high magnification SE SEM image.

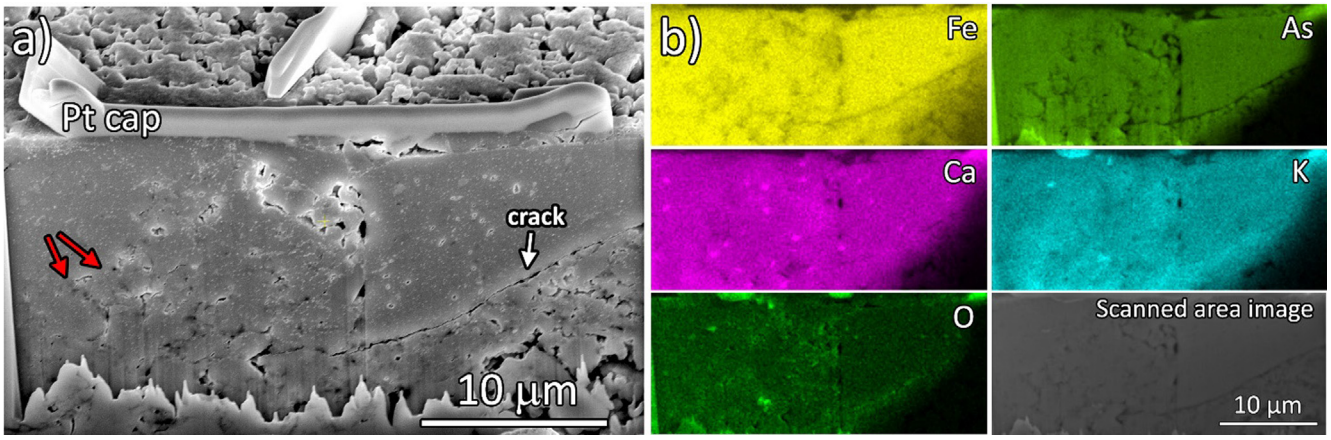

Fig. 3. (a) Secondary electron through-the-lens (TLD) SEM image on the surface of a freshly synthesized pellet as reported in Fig. 2 after 20 mm depth cross sectional FIB'ing (focused ion beam) and (b) X-ray energy dispersive spectroscopy (EDS) maps of Fe, As, Ca, K, and O elements of the cross section.

analyses carried out on thin lamellae extracted out by FIB in order to enhance the spatial resolution of EDS measurements avoiding the bulk contribution to the EDS signals are reported in the Supporting Information. It is observed that while iron and arsenic are homogeneously distributed across the compound, higher variability is evidenced for calcium, potassium, and oxygen elements. Looking at the oxygen picture, apart from an enrichment on the surface, it is observed that its concentration increases at the aggregates boundaries. This well copes with the distribution of potassium and calcium, quite homogeneous inside the aggregates, with signal enhancements evident at grain boundaries. The behavior of the alkaline and alkaline-earth element is however different: while calcium segregates at the aggregates boundaries in the form of discrete particles, potassium distribution seems more widespread. The calcium segregation is likely to represent calcium oxide, while potassium enrichment could be related to the presence of the K-122 phase, both commonly observed by XRD diffraction as minor contaminants in these samples [16].

The same analyses sequence was carried out on oxidized pellets. In Fig. 4a is reported the surface morphology of a pellet exposed to air for 24 h. No significant differences with respect to the pristine sample are noticeable apart from a slightly increased roughness of the dense aggregates and a slight smoothening of the large crystal's edges. These aspects are further enhanced for longer exposure time, as evident in Fig. 4b, where the microstructure of a sample exposed to air for

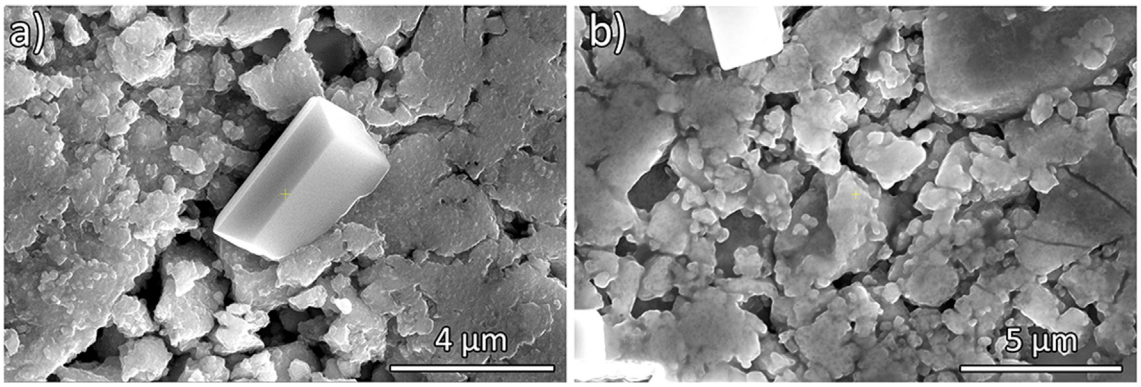

Fig. 4. Secondary electron SEM images of the sample surface after (a) 24 h and (b) 3.5 weeks of air exposure.

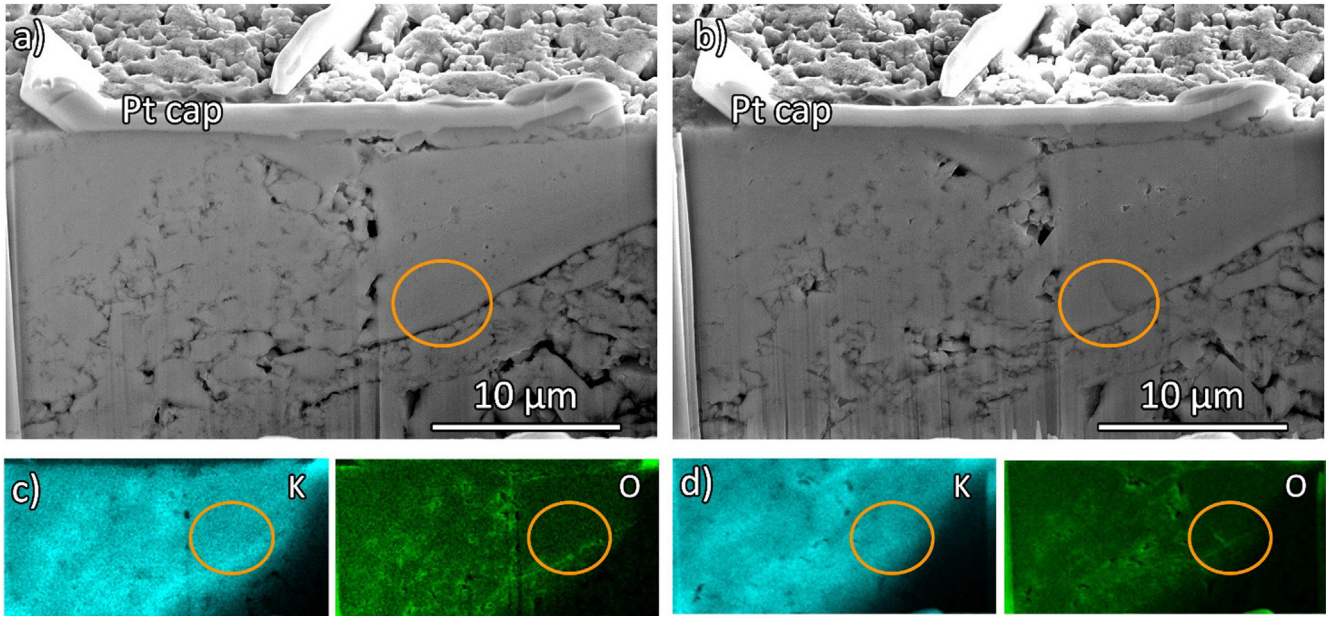

Fig. 5. (a,c) SEM images and EDS mapping for Potassium and Oxygen of the sample section depicted in Fig. 3 after 3.5 weeks of air exposure; (b,d) the same sample section after removal of the oxidized layer (see text for details).

3.5 weeks is reported. As evident from the images, a general blurring of the surface is evident.

The bulk structure evolution was assessed by observing the same pristine sample section after exposure to air for 3.5 weeks. The image and the EDX maps are reported in Fig. 5a. With respect to the pristine sample, a slight enrichment in the oxygen content can be observed on the whole section surface, suggesting that the surface of the section milled by the FIB has been oxidized. Considering the SEM/EDS limitations in the quantitative analysis of light elements such as oxygen, we limited our analysis to a qualitative comparison. In order to enhance this oxygen evolution, the section was further milled for approximately 0.5 μm in order to expose and examine inner layers of the air exposed compound. The results are depicted in Fig. 5b. With respect to the analysis prior to the additional milling (Fig. 5a) it can be clearly observed that oxygen signal from the dense aggregates tends to decrease, remaining instead well evident and concentrated at the aggregate boundary. This suggests that the sample surface evenly oxidizes, and that oxygen diffuses in the sample bulk following preferential pathways, the boundaries of the dense aggregates. The porous volume tends thus to represent a highway for oxygen diffusion, allowing oxidation of the compound otherwise masked. Further evidence is provided by the detail highlighted in the orange circle, that depicts the aggregate before and after the second material removal: the appearance of a crack buried in the aggregate, not evident in the first analysis, is accompanied by the appearance of oxygen in the EDS maps.

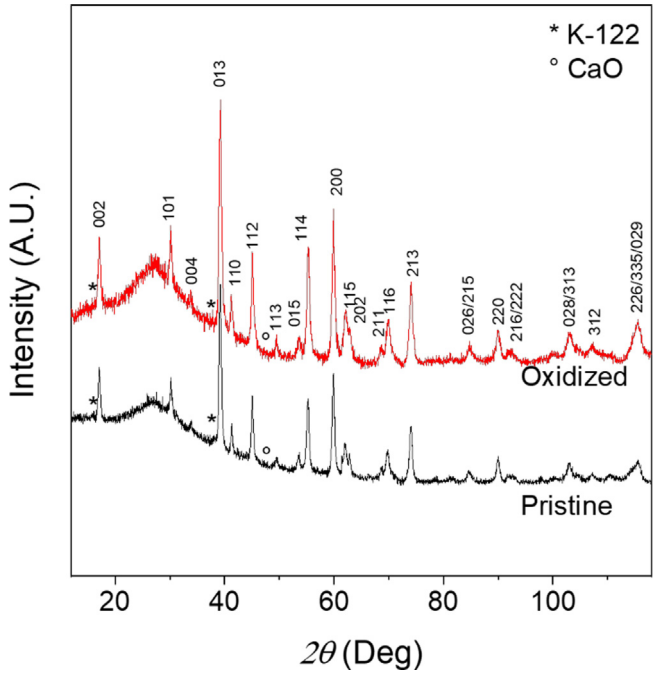

Fig. 6. XRD patterns of pristine and oxidized samples (3.5 weeks in air); main peaks are indexed for the Ca/K P4/mmm phase, and symbols refer to the position of K-122 and CaO main reflections.

The microscopical investigation suggests thus that the bulk morphological properties of the compound and its average chemical composition are not affected by the oxidation process that is mainly confined at the aggregates boundaries.

To verify phase stability, the XRD pattern of an oxidized sample was collected as shown in Fig. 6, in comparison with the pristine reference. No large differences are observed and no peaks ascribable to secondary phases, that could suggest a significant structural change, appear in the pattern.

The significant degradation in the superconducting behavior is however confirmed by means of magnetic measurements. The magnetic hysteresis loop measured at 4.2 K for a sample exposed to air for 1 h is reported in Fig. 7. Contrarily to the pristine samples [16], the curve is characterized by a significant asymmetry, with a reverse sigmoidal shape, zero-field peaks shifted with respect to the zero magnetic field, and a significant reversible background. These features, most likely related to granularity phenomena [17], suggest that the effective current transfer across the sample is inhibited following the air exposure. This is confirmed by the estimation of critical current density by means of Beans model [15], that results in values of approximately 2.5 $\times$ 10^3 A/cm^2 in self-field that falls to approximately 500 A/cm^2 at 5 T, more than one order of magnitude lower with respect to the pristine sample.

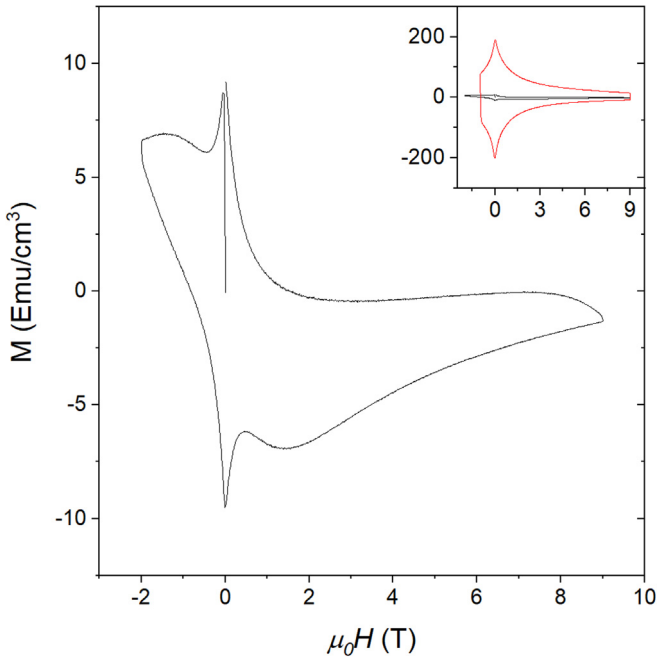

Fig. 7. Magnetic hysteresis loop measured at 4.2 K for a sample exposed in air for 1 h. In the inset, a comparison with a pristine sample (in red).

Considering that the crystalline structure of the sample seems not to be significantly affected by the air exposure, while the transport of the superconducting currents across the whole sample is significantly hindered, the investigation of the superconducting properties of the material by means of an appropriate intragrain technique, such as the measurement of specific heat, is mandatory to assess if the whole superconducting compound is affected by the oxidation phenomenon, leading to a worsening of the intrinsic superconducting properties. In Fig. 8 the measurements carried out at zero and 10 T field in the temperature range of 2–45 K are reported for the pristine sample and a sample oxidized for 24 h. The specific heat ($C/T = \gamma_n$) at normal state is obtained by fitting with $C/T = \gamma_0 + \beta T^2$. The C/T plots show a sharp and clear onset transition near 35 K in the absence of magnetic field and slightly shifted to lower temperature when 10 T magnetic field is applied, for both cases of the pristine and oxidized samples. Interestingly, no significant difference is observed between the two samples, and this feature is more obvious in the plot of $\gamma - \gamma_n$ in Fig. 8b.

Observing the evolution of the material properties following the exposure to air, it is straightforward to suppose that the degradation of the superconducting properties is due to granularity phenomena rather than to the decomposition of the superconducting compound, at least for the timescale investigated. To assess in detail this aspect, a deeper microscopical characterization was carried out. A detailed analysis of the sample microstructure is reported in Fig. 9, depicting the BF-STEM images acquired on a lamella obtained from a sample exposed to air for 3.5 weeks. Starting from the low magnification image (panel a), the analysis allows to observe the presence of a limited amount of well-evident clear grain boundaries - tens of nanometers thick - across the sample, and several white particles. It is straightforward to identify this thick grain boundaries with the boundaries of the aggregates evident by means of SEM images, where oxide tend to concentrate, and the globular particles with calcium oxides. Going more in detail (Fig. 9b) inside the aggregates, it is evidenced how the compound is formed by elongated grains of homogeneous dimensions, few tens of nanometers on the short side and 100–200 nm along the long direction. EDS mapping, reported in Fig. 9c, confirms these assessments, with a homogeneous dispersion of iron and arsenic elements, while oxygen is concentrated at the aggregate boundaries and in the calcium rich globular particles. Finally, a fine investigation of grain boundaries inside the aggregates, reported in the Fig. 9b, allows to observe a brighter layer few nanometers thick most likely associated with oxygen presence (Fig. 9d).

High angular dark field (HAAF) images were acquired in addition to STEM bright field image, as shown in Fig. 10. In the panel a grain structures with different crystalline orientations separated by a ~20 nm thick grain boundary are reported. Based on FFT patterns shown in Fig. 10b and Fig. 10c, it is found that grain I is tilted along [0 0 1] direction while grain II is projected along [1 1 0] direction. Additionally, the grain boundary is very wide (~20 nm) and shows amorphous features. Atomic resolution HAADF image in Fig. 10d corresponds to grain II tilted along [1 1 0] direction, which clearly reveals the stacking of Fe, As, Ca and K layers along the [0 0 1] direction. From these images, it can be observed that the crystalline compound is characterized by a highly ordered structure, with the regular arrangement characteristic of the 1144 phase. The grain boundary, on the contrary,

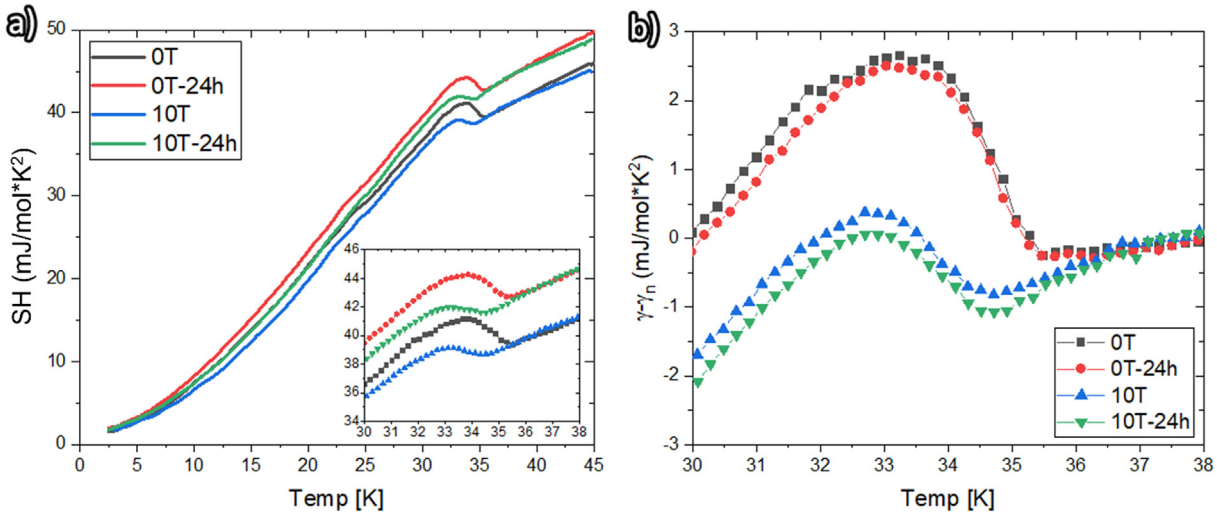

Fig. 8. Volumetric specific heat (SH) vs temperature plots of pristine and 24 hours oxidized samples at zero and 10 T magnetic field. (a) C/T vs T with a inset for T_c transtion, and (b) γ- γ_n vs T plots.

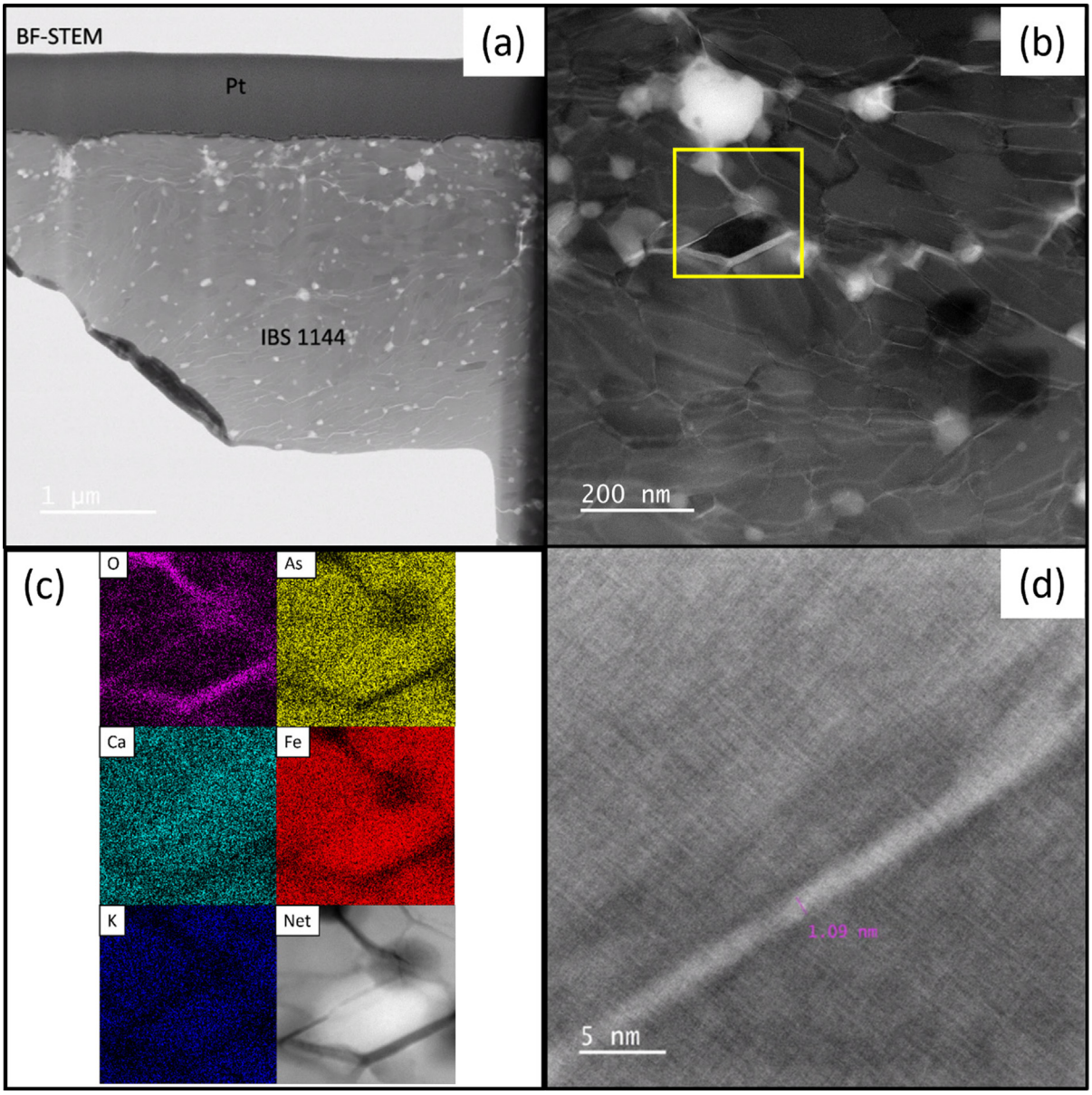

Fig. 9. BF-STEM (Bright Field – Scanning Transmission Electron Microscopy) image of a 1144 lamella from a 3.5 weeks air exposed pellet (a), with details of the grain structure (b), EDS mapping of the highlited area (c) and enlarged view of a grain boundary (d).

does not show evidence of a regular crystalline structure, suggesting thus an amorphous layer.

4. Discussion

The formation of blocking layers at grain boundaries in IBSC is a crucial issue, to be solved in order to unlock the full potential of this class of materials. Previous studies have observed the formation of amorphous or crystalline oxygen contaminated layers at grain boundaries during the material synthesis (e.g. [18–20]), testifying the detrimental effect on the superconducting properties.

The effect of the aging of these materials, and thus of the modification of the compound after the synthesis thermal process, is however a rarely studied aspect crucial in view of the potential large-scale application. From this point of view, our experimental results on the effect of the oxidation on Ca/K-1144 compounds can be compared to similar studies carried out on Ba/K-122 compounds [21]. In this recent work by Tu et al. [21], it is shown that Ba/K-122 polycrystalline compounds immersed in water tend to form on the surface a series of corrosion layers involving the initial formation of hydroxides and their conversion in carbonates, eventually working as a passivation layer. Despite being our exposure conditions less severe (humid air vs liquid water), it is likely to suppose that similar processes are ongoing also for Ca/K-1144 compounds.

Taking into account such results, we decided to assess if the atmosphere composition could play a role in the loss of a percolative path for the supercurrents in the sample. The material was thus exposed to a different environment, i.e. pure oxygen. In Fig. 11 it is reported the resistive transition of a pristine sample in comparison with a sample kept in a pure oxygen atmosphere for 3 months (full symbols). As we can observe, after 3 months in pure oxygen, the samples are characterized by a limited decrease of the zero resistance critical temperature, not at all comparable with the critical temperature decrease observed when exposing the samples to ambient air. We would additionally like to mention that to insert the pellets in the pure oxygen vial, a short passage in ambient air was necessary, and thus a possible minor contamination could be involved in this first step. Following the measurement, the same sample previously exposed to pure oxygen was exposed for 2 additional hours to humid air, and this caused a signif-

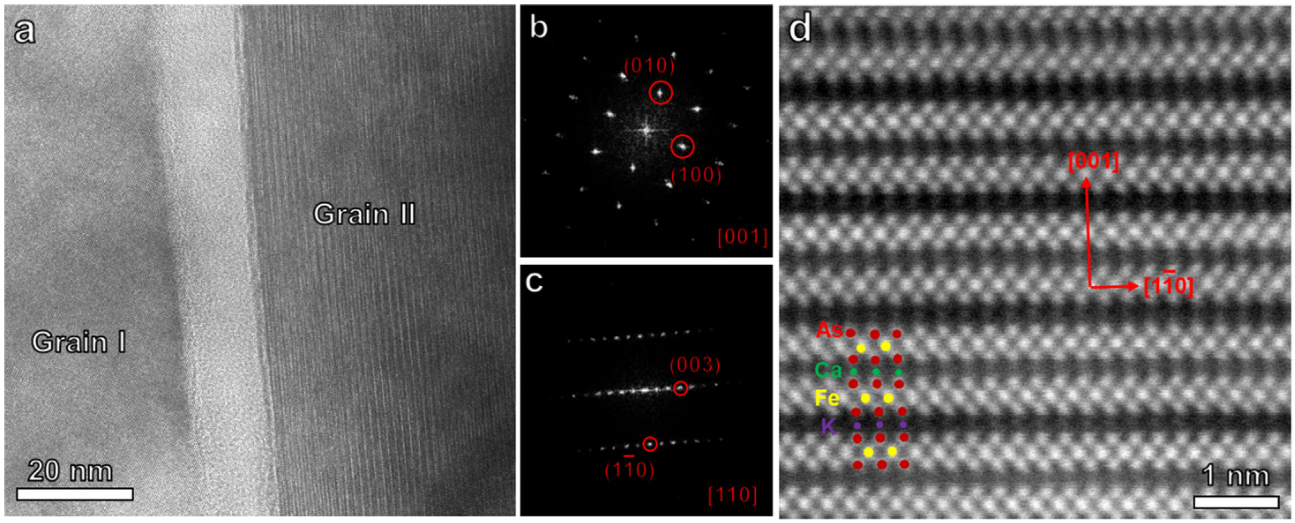

Fig. 10. (a) High resolution TEM image depicting two crystallites characterized by different orientations and a thick grain boundary. (b, c) Fast Fourier transformed (FFT) patterns corresponding to grain I and II indicated in (a). (d) Atomic resolution HAADF imaging of grain II. Inset red, yellow, purple, and green balls represent the atomic layer of As, Fe, K and Ca respectively.

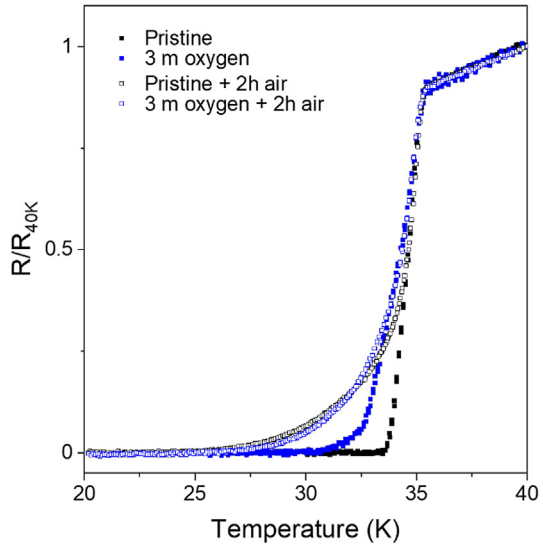

Fig. 11. Resistive transition for a pristine compound and a sample kept in oxygen for 3 months, and the same samples exposed in air for 2 h.

icant broadening of the resistive transition (empty symbols). This means that a significant degradation is caused by exposure of the sample to humid air, much more severe than that induce by pure oxygen. Considering this, however, further studies will be carried out focused on the assessment of the different contaminant's role on the degradation of the grain boundary in Ca/K-1144. These preliminary measurements already suggest however that oxygen may not be the main culprit for the degradation of Ca/K-1144 samples, but water and carbon dioxide may be accounted for the loss of grain connectivity with mechanisms similar to the one proposed for the Ba/K-122 samples. In this sense, it seems crucial to avoid the exposure of Ca/K-1144 compounds to humidity.

With respect to Ba/K-122 compounds, however, we observe a significant difference in the oxidation behavior. The work by Tu et al. [21] shows indeed a passivation mechanism on the surface of the pellets, with superconducting behavior retained by the bulk of the samples. In our case, instead, the superconducting performance is promptly lost upon oxidation. As in Tu's work, however, decomposition of the bulk structure does not take place, but rather a deterioration at the GBs. Considering the mechanisms proposed in their work, involving the formation of hydroxides, and the similar expected behavior of calcium and barium ions in oxidizing media, it is likely to not ascribe the different response of the 1144 phase with respect to the 122 compound just to the chemical composition. On the contrary, the microstructure of the compound is expected to significantly influence the performance loss upon oxidation. Open porosity is expected in particular to play a crucial role in the oxidation behavior of the sample, allowing for oxidizing species to diffuse deep in the materials bulk.

The existence, for oxidizing species, of diffusion pathways in the polycrystalline samples is most likely correlated also to the presence on the surface and porosities of the large crystals (see SEM images and our previous works [16]). These crystals are never observed when milled powders are processed at low temperature (500 °C) [16], while they appear after thermal treatments at higher temperature (>650 °C) meaning that their growth is not related to the mechanochemical step. Moreover, the growth of such crystals is unlikely due to sintering phenomena and related Ostwald ripening, because in such case it should occur inside the aggregates, where density is higher. Instead, the appearance of such large single crystals on the surface and in porosities suggests that is most likely due to vapor phase transport phenomena. SEM/EDS measurements - confirmed also by the TEM analyses, suggest that the open porosity around the aggregates–constitutes a preferential channel both for the diffusion of volatile species during thermal processing and oxidizing agents. Such porosity originates from the milling step - well known to lead to the formation of such structures [22], and countermeasures should be enacted to avoid/minimize such occurrence.

Critical temperature of 1144 polycrystalline compounds, and Ca/K-1144 in particular, has been always related to their stoichiometric chemical composition, and considered invariant and robust towards doping and chemical inhomogeneity. In reality, a certain degree of variation has been always observed between the different research groups involved in the synthesis of these compound: for example, in the first work from Iyo et al. it is shown a resistive transition with the onset at approximately 33 K and zero resistance at approximately 32 K [8]. Following works show some variability with higher onset (i.e. 33.8 K [23] or 35 K [24]), and broader transitions, in particular for samples processed at atmospheric pressure, while highly dense samples processed with Spark Plasma Sintering are characterized by extremely sharp transitions [24]; Onset at approximately 35 K and zero resistance values towards 30 K have been shown by Cheng et al. [25], and values

of approximately 34 K and 31 K have been obtained by Singh et al. [26] While light differences in the onset values may be due to the different testing facilities, and possibly also due to small differences in the lattice structure as suggested in previous works [27], the large difference in the transition width is likely due to extrinsic factors. As reported in this work, oxidation of the pristine compound leads to a broadening of the superconducting transition most likely associated to the introduction of weak links at grain boundaries, reflected in the loss of zero-resistance critical temperature. Our results may explain the large variability observed in literature for CaK-1144 compounds: a strict correlation between exposure time and critical temperature is however not straightforward considering the variables involved in the phenomenon. With respect to works from other groups, where the synthesis is carried out at high temperature, our compound is characterized by crystallite size at least one order of magnitude lower [23,25,26], or significantly different densities (e.g. [24]) and this could significantly influence the oxidation pathways. As a general impression, however, improvement of density seems a critical topic that should be pursued in order to inhibit the diffusion of oxidants in the bulk of the material.

5. Conclusions

The morpho-structural characteristics and superconducting properties evolution of Ca/K-1144 polycrystalline samples following the exposure in air and pure oxygen is reported. Oxidation of grain boundaries concentrated around open porosities leads to a loss of percolative pathways for the superconducting currents, with a significative decrease of the superconducting zero-resistance critical temperature and of the critical currents. However, the bulk structure of the compound, investigated by means of high-resolution STEM, is not affected, as confirmed also by specific heat measurement that do not show signs of degradation of the superconducting bulk properties.

These results suggest that loss of superconducting properties in Ca/K-1144 compounds that follows oxidation is mainly due to a worsening of grain boundary current transfer phenomena, and not related to structural phase degradation. A role of the oxidizing agent is furthermore identified, with water most likely playing a major role in the performance degradation.

In conclusion, it seems thus crucial to avoid the exposure of polycrystalline 1144 compounds to oxidizing atmospheres in order to preserve a good grain connectivity and thus percolative pathways for superconducting currents.

Declaration of Competing Interest

The authors declare that they have no known competing financial interests or personal relationships that could have appeared to influence the work reported in this paper.

Acknowledgements

Part of the work was carried out in the framework of the Cooperative Research And Development Agreement CRADA FRA-2022-0041. This work made use of the EPIC facility of Northwestern University's NUANCE Center, which has received support from the SHyNE Resource (NSF ECCS-2025633), the IIN, and Northwestern's MRSEC program (NSF DMR-1720139).

Appendix A. Supplementary material

Supporting Information Available: SEM/EDS images of FIB lamellae and SEM/EDS images and EBSD patterns of large single crystals and the pellets surface. Supplementary data to this article can be found online at https://doi.org/10.1016/j.supcon.2023.100062.

References

[1] Hosono H, Yamamoto A, Hiramatsu H, Ma Y. Recent advances in iron-based superconductors toward applications. Mater Today 2018;21:278–302. https://doi.org/10.1016/j.mattod.2017.09.006.
[2] Zhang X, Ma Y. Progress in the development of the 122-type IBS wires. Superconductivity 2022;2:100010. https://doi.org/10.1016/j.supcon.2022.100010.
[3] Yao C, Ma Y. Recent breakthrough development in iron-based superconducting wires for practical applications. Supercond Sci Technol 2019;32:023002. https://doi.org/10.1088/1361-6668/aaf351.
[4] Guo W, Yao C, Huang H, Dong C, Liu S, Wang C, et al. Enhancement of transport J c in (Ba, K)Fe_2As_2 HIP processed round wires. Supercond Sci Technol 2021;34:094001. https://doi.org/10.1088/1361-6668/ac1952.
[5] Li W, Huang H, Guo C, Tu C, Liu X, Yao C, et al. Significant enhancement of transport J_c in Cu/Ag-sheathed (Ba, K)Fe_2As_2 superconducting tapes by pre-composite technique. Sci China Mater 2022:1–10. https://doi.org/10.1007/s40843-022-2159-1.
[6] Lin H, Yao C, Zhang X, Zhang H, Zhang Q, Wang D, et al. Effect of metal (Zn/In/Pb) additions on the microstructures and superconducting properties of $Sr_{1-x}K_xFe_2As_2$ tapes. Scr Mater 2016;112:128–31. https://doi.org/10.1016/j.scriptamat.2015.09.031.
[7] Pak C, Su Y-F, Collantes Y, Tarantini C, Hellstrom EE, Larbalestier DC, et al. Synthesis routes to eliminate oxide impurity segregation and their influence on intergrain connectivity in K-doped $BaFe_2As_2$ polycrystalline bulks. Supercond Sci Technol 2020. https://doi.org/10.1088/1361-6668/aba01a.
[8] Iyo A, Kawashima K, Kinjo T, Nishio T, Ishida S, Fujihisa H, et al. New-Structure-type Fe-Based superconductors: $CaAFe_4As_4$ (A = K, Rb, Cs) and $SrAFe_4As_4$ (A = Rb, Cs). J Am Chem Soc 2016;138:3410–5. https://doi.org/10.1021/jacs.5b12571.
[9] Ichinose A, Pyon S, Tamegai T, Ishida S. Elucidating the origin of planar defects that enhance critical current density in $CaKFe_4As_4$ single crystals. Supercond Sci Technol 2021;34:034003. https://doi.org/10.1088/1361-6668/abdba7.
[10] Pyon S, Miyawaki D, Veshchunov I, Tamegai T, Takano K, Kajitani H, et al. Fabrication and characterization of $CaKFe_4As_4$ round wires sintered at high pressure. Appl Phys Express 2018;11:123101. https://doi.org/10.7567/APEX.11.123101.
[11] Cheng Z, Liu S, Dong C, Huang H, Li L, Zhu Y, et al. Effects of core density and impurities on the critical current density of $CaKFe_4As_4$ superconducting tapes. Supercond Sci Technol 2019;32:105014. https://doi.org/10.1088/1361-6668/ab3a87.
[12] Masi A, Angrisani Armenio A, Augieri A, Celentano G, Duchenko A, Rufoloni A, et al. Cu/Ta sheaths for iron-based superconductors: First experimental findings in Ca/K-1144 wires. Superconductivity 2022;2:100014. https://doi.org/10.1016/j.supcon.2022.100014.
[13] Masi A, Angrisani Armenio A, Celentano G, La Barbera A, Rufoloni A, Silva E, et al. Mechanochemically assisted low temperature synthesis route of the 1144 Ca-K Iron Based Superconductor. Supercond Sci Technol 2020;33:074003. https://doi.org/10.1088/1361-6668/ab9029.
[14] Masi A, Angrisani Armenio A, Augieri A, Celentano G, Fiamozzi Zignani C, La Barbera A, et al. Superconducting properties of 1144-type iron-based superconductors by mechanochemically assisted synthesis. MRS Adv 2021. https://doi.org/10.1557/s43580-021-00151-9.
[15] Bean CP. Magnetization of high-field superconductors. Rev Mod Phys 1964;36:31–9. https://doi.org/10.1103/RevModPhys.36.31.
[16] Masi A, Angrisani Armenio A, Celentano G, La Barbera A, Rufoloni A, Silva E, et al. The role of chemical composition in the synthesis of Ca/K-1144 iron based superconductors. J Alloy Compd 2021;869:159202. https://doi.org/10.1016/j.jallcom.2021.159202.
[17] Passos WAC, Lisboa-Filho PN, Caparroz R, De Faria CC, Venturini PC, Araujo-Moreira FM, et al. Granularity in superconductors: Intrinsic properties and processing-dependent effects. Physica C (Amsterdam, Neth) 2001;354:189–96. https://doi.org/10.1016/S0921-4534(01)00045-4.
[18] Wang L, Ma Y, Wang Q, Li K, Zhang X, Qi Y, et al. Direct observation of nanometer-scale amorphous layers and oxide crystallites at grain boundaries in polycrystalline $Sr_{1-x}K_x$ Fe_2As_2 superconductors. Appl Phys Lett 2011;98. https://doi.org/10.1063/1.3592580.
[19] Kim YJ, Weiss JD, Hellstrom EE, Larbalestier DC, Seidman DN. Evidence for composition variations and impurity segregation at grain boundaries in high current-density polycrystalline K- and Co-doped $BaFe_2As_2$ superconductors. Appl Phys Lett 2014;105. https://doi.org/10.1063/1.4898191.
[20] Kametani F, Su YF, Collantes Y, Pak C, Tarantini C, Larbalestier D, et al. Chemically degraded grain boundaries in fine-grain $Ba_{0.6}K_{0.4}Fe_2As_2$ polycrystalline bulks. Appl Phys Express 2020;13. https://doi.org/10.35848/1882-0786/abbfdf.
[21] Tu C, Dong C, Yao C, Yang P, Guo W, Zhang Q, et al. Robust superconductivity against water corrosion in $Ba_{1-x}K_xFe_2As_2$ bulks. Supercond Sci Technol 2021;34:125008. https://doi.org/10.1088/1361-6668/ac30ce.
[22] Avakumov E, Senna M, Kosova N, Avvakumov E, Senna M, Kosova N. Soft mechanochemical synthesis. Boston: Kluwer Academic Publishers; 2001. https://doi.org/10.1007/b114163.
[23] Sugali PKN, Ishida S, Kimoto K, Yanagisawa KK, Kamiya Y, Tsuchiya Y, et al. Intrinsic defect structures of polycrystalline $CaKFe_4As_4$ superconductors. Phys Chem Chem Phys 2021;23:19827–33. https://doi.org/10.1039/D1CP02613E.
[24] Ishida S, Pavan Kumar Naik S, Tsuchiya Y, Mawatari Y, Yoshida Y, Iyo A, et al. Synthesis of $CaKFe_4As_4$ bulk samples with high critical current density using a

spark plasma sintering technique. Supercond Sci Technol 2020. https://doi.org/10.1088/1361-6668/aba019.
[25] Cheng Z, Dong C, Huang H, Liu S, Zhu Y, Wang D, et al. Chemical stability and superconductivity in Ag-sheathed $CaKFe_4As_4$ superconducting tapes. Supercond Sci Technol 2019;32:015008. https://doi.org/10.1088/1361-6668/aaedff.
[26] Singh SJ, Cassidy SJ, Bristow M, Blundell SJ, Clarke SJ, Coldea AI. Optimization of superconducting properties of the stoichiometric $CaKFe_4As_4$. Supercond Sci Technol 2020;33:025003. https://doi.org/10.1088/1361-6668/ab58be.
[27] Masi A, Duchenko A, Celentano G, Varsano F. Tailoring the critical temperature of Ca/K-1144 superconductors: the effect of aliovalent substitution on tetragonality. Supercond Sci Technol 2022. https://doi.org/10.1088/1361-6668/ac6630.